

Synthesis and Characterization of the Magnetically Separable Composite of Iron Oxide and Graphitic Carbon Nitride for Degradation of Methylene Blue

Nur Aisyah Mohamad Azali, Norazila Abdul Rahman, Rozaina Saleh, Mazlini Mazlan and Nurul Izza Taib*

Faculty of Applied Sciences, Universiti Teknologi MARA, Perak Branch, Tapah Campus, 35400 Tapah Road, Perak, Malaysia

*Corresponding author (e-mail: izza257@uitm.edu.my)

Magnetic composite of magnetite (Fe_3O_4) and graphitic carbon nitride (g- C_3N_4), labeled as S4 and S5, respectively, were synthesized using a co-precipitation method starting from Fe^{2+} and Fe^{3+} salts and g- C_3N_4 , which was obtained by different starting nitrogen-rich organic precursors; urea and mixture of melamine and urea by thermal polymerization. The composites were tested for methylene blue (MB) degradation in an aqueous solution under visible light irradiation. The physicochemical properties of the composites were characterized by XRD, FTIR, SEM-EDX, CHNS Analyzer, UV-Vis diffuse reflectance absorption spectra (UV-Vis DRS), and VSM. The magnetic composite S4 and S5 enable 68.9% and 90.9% degradation of MB within 5 hours, respectively. This study demonstrates that the photocatalytic methylene blue under visible light is approximately two times greater when a mixture of urea and melamine is used as the g- C_3N_4 precursor than urea alone. Furthermore, the composite's high saturation magnetization suggests that the photocatalyst can be easily separated from the treated solution using a magnetic field.

Keywords: Graphitic carbon nitride; iron oxide; methylene blue; $\text{C}_3\text{N}_4/\text{Fe}_3\text{O}_4$; photocatalyst; magnetic

Received: August 2022; Accepted: October 2022

The massive production and widespread use of synthetic dyes in textiles, paper, food additives, and other industries have experienced tremendous growth. They have significantly polluted the aquatic system [1] and harmed human and animal health even at low concentrations [2, 3]. It also reduces light transmission in contaminated water and causes aquatic life to run out of oxygen [2]. Therefore, the removal of synthetic dyes is becoming increasingly important. Semiconductor photocatalysis is known to be an effective technology to combat such pollutants [4, 5].

In this regard, graphitic carbon nitride (g- C_3N_4), constituted of the elements C and N, has received numerous attention as a polymeric compound photocatalyst for organic pollutant degradation [6-8]. g- C_3N_4 is a robust and stable visible-light-driven photocatalyst with a medium-bandgap of 2.7 eV, nontoxicity, has strong chemical stability with an attractive electronic structure [9, 10] emerges as a good candidate for the photocatalytic process. g- C_3N_4 has been synthesized using several methods, including thermal polymerization [11, 12], solvent sonochemical [13], template-directed solid-state [14], and so on. It is important to note that g- C_3N_4 can be easily synthesized thru a one-step method from cheap precursors such as cyanamide, dicyandiamide, melamine, thiourea,

and urea. Nonetheless, g- C_3N_4 alone suffers some withdrawal, such as rapid recombination of photo-generated charge carriers and poor absorption in the visible region, resulting in low photocatalytic activity under visible-light illumination [15-17].

Recently, doping with metallic or nonmetallic materials, increasing surface area, and combination with other semiconductors have been used to enhance the photocatalytic activity of g- C_3N_4 [12]. Because of their high saturation magnetizations [18, 19], Fe_3O_4 nanoparticles are a popular choice. Since g- C_3N_4 is non-magnetic, it can't be easily recycled or separated from treated solutions using an external magnetic field, causing secondary contamination. Thus, loading magnetic materials such as Fe_3O_4 on g- C_3N_4 is an excellent option for extracting photocatalysts from photocatalytic systems [20, 21].

Kowitsch et al. [22] reported the use of iron oxides-carbon nitride materials under visible light irradiation, and the degradation rate of an aqueous rhodamine B (RhB) solution in composites was evaluated. The magnetic composite $\alpha\text{-Fe}_2\text{O}_3(3\%)/\text{CN}$ permits 82% RhB degradation in 90 minutes. Christoforidis et al. [23] synthesized metastable $\beta\text{-Fe}_2\text{O}_3$ nanoparticles on g- C_3N_4 using a solid-state, in-situ growth

technique. The incorporated β -Fe₂O₃ improves the photocatalytic activity by improving visible light absorption and carrier separation. The composite β -Fe₂O₃(3.5 ω)/CN shows a methyl orange degradation of 80% in 4 hours, whereas the degradation rate with pure β -Fe₂O₃ is only about 5%. Kheradmand et al. [24] reported the impregnation of Fe₂O₃ and Fe₃O₄ on C₃N₄ nanotubes (NTs) for visible-light hydrogen production. Fe₃O₄/C₃N₄ NTs with 3% Fe₃O₄ mass content had 1.9-fold the photocatalytic activity of bare C₃N₄ NTs. The better activity of Fe₃O₄/C₃N₄ NTs compared to Fe₂O₃/C₃N₄ NTs can be attributed to the increased use of visible-light radiation and efficient electron–hole pair separation, which leads to a decreased recombination rate.

Numerous studies have been conducted on the preparation of g-C₃N₄-related co-catalysts. However, comparative studies on the synthesis of their starting materials are scarce. Melamine, an organic nitrogen heterocyclic triazine, was the typical substance used to generate g-C₃N₄. Urea, readily available with the chemical formula (NH₂)₂CO, was considered a green precursor for g-C₃N₄. Due to their nitrogen-rich nature, melamine and urea have been proven to be active precursors for producing g-C₃N₄.

In this work, two types of g-C₃N₄ were synthesized using different precursors, (i) urea and (ii) a mixture of urea and melamine, which were then loaded with Fe₃O₄. The precursors were processed simultaneously under similar conditions via thermal polymerization. The objective was to systematically compare the structure and properties of g-C₃N₄ generated from various raw materials. Importantly, no templates or additional solvents were required for synthesis, making this method far more environmentally friendly than others. The synthesized samples were characterized using XRD, FTIR, SEM-EDX, CHNS Analyzer, UV-Vis diffuse reflectance absorption spectra (UV-Vis DRS), and VSM. Then, the magnetic composites were explored regarding the photocatalytic performance under visible light irradiation.

EXPERIMENTAL

Chemicals and Materials

In this work, the fresh leaves of *Azadirachta indica* (neem leaves) were collected from Tapah Road, Perak, Malaysia. Iron (II) chloride tetrahydrate (FeCl₂·4H₂O), iron (III) chloride hexahydrate (FeCl₃·6H₂O), ammonium hydroxide (NH₄OH), Urea, and Melamine were purchased from R&M Chemicals. Methanol was obtained from Sigma Aldrich Chemical Company. For the dye, methylene blue (MB) as a model pollutant was purchased from R&M Chemicals. All chemicals were of analytical grade and utilized without further purification.

Characterization Methods

Instruments

X-ray powder diffraction (XRD) was used to analyze the structure and identify the phase purity of samples. The samples were placed on a flat plate while intensity data were collected as a function of the Bragg angle, θ , in the range $2\theta = 15^\circ$ to 80° with a step size of 0.013° using a PANanalytical X'pert PRO diffractometer in Bragg–Brentano geometry using Cu K_α radiation wavelength $\lambda_{\alpha 1} = 1.5405 \text{ \AA}$, $\lambda_{\alpha 2} = 1.5443 \text{ \AA}$. Attenuated total reflection-Fourier transform infrared (ATR-FTIR) spectroscopy (Perkin Elmer spectrum one spectrophotometer) in transmission mode with a spectrum range of $4,000$ to 550 cm^{-1} and a resolution of 4 cm^{-1} was used to study the functional groups of samples. A CHNS analyzer was used to perform their elemental analysis (Thermo Scientific, Flash 2000). A Benchtop Scanning Electron Microscope (BSEM) attached with Energy Dispersive X-ray (EDX) analyzer was used to examine their surface morphology (Phenom XL). The magnetic properties were measured using a vibrating sample magnetometer (VSM, Lake Shore 7404, McCorkle Boulevard, Westerville, OH, USA) at room temperature 300 K. The magnetization measurements, M_s as a function of the applied field (H), were measured under external magnetic fields up to $\pm 20,000 \text{ Oe}$. The absorbance from photocatalytic degradation of MB was analyzed using UV-Visible spectroscopy (PerkinElmer Lambda 35) at $\lambda_{max} = 664 \text{ nm}$ wavelength.

Preparation of *Azadirachta indica* (Neem Leaves) Extract

The healthy leaves of *Azadirachta indica* (neem leaves) were collected from Tapah Road, Perak, Malaysia. The collected leaves were thoroughly washed several times with distilled water to remove dust particles and then air dried at room temperature to remove the remaining moisture. Then, the dried leaves were cut into small pieces and crushed into fine powder. Approximately 5 g of finely grinded neem leaf powder was mixed with 100 mL of sterile distilled water in a conical flask, and the mixture was heated up for 30 minutes at a constant temperature of 80°C . The mixture was heated on a hot plate and continuously stirred with a magnetic stirrer to ensure that the mixture was homogeneous. Then, the mixture was left to cool at room temperature before being vacuum-filtered through Whatman filter paper No. 1 to obtain plant extract. The green clear filtered extract solution was stored at 4°C for further use [25, 26]. The extract solution can be kept for up to a month at 4°C .

Preparation of g-C₃N₄

Urea and melamine were used as the precursor materials in the thermal polymerization method to

prepare graphitic carbon nitride (g-C₃N₄ [27, 28]. 10 g of urea powder was weighed and placed in a crucible with a lid. The sample was heated up to 550 °C for 3 hours using a heating rate of 5 °C/min in a furnace. The obtained yellow product was cooled down to room temperature and grinded in a mortar into powder. The samples were denoted as S1. The same procedures were repeated using the mixture of 3 g of urea and 7 g of melamine powder as the precursor, and the samples were denoted as S2.

Co-Precipitation of Iron Oxide Nanoparticles (Fe₃O₄-NPs)

Neem leaf extract was used to prepare iron oxide nanoparticles as the reducing and stabilizing agent. Iron Oxide nanoparticles (Fe₃O₄-NPs) were prepared using co-precipitation according to a published procedure [25]. 1.10 g of iron (III) chloride hexahydrate and 0.40 g of iron (II) chloride tetrahydrate with a 1:2 molar ratio were weighed and dissolved in 100 mL of distilled water. The solution was transferred into the round bottom flask, and the resultant mixture was heated for 10 minutes at 80 °C under a nitrogen blanket. Then, 5 mL of aqueous neem leaf extract was added slowly to the resulting hot solution. Then, 20 mL of 25% ammonium hydroxide (NH₄OH) was added drop by drop into the solution for 30 minutes while vigorously stirring. The colour of the mixture instantly changed to the black colour solution, indicating the formation of Fe₃O₄-NPs. The mixture was allowed to cool at room temperature for 30 minutes until the dark precipitate settled to the bottom of the flask. After the supernatant was discarded, the remaining black precipitate was rinsed with 15 mL distilled water. The washed precipitate was centrifuged for 5 minutes at 8500 rpm, and then the pellet was dried in the oven at 60 °C for 8 hours after the supernatant was removed. Afterward, the obtained black product was ground in a mortar and kept at room temperature. The samples were denoted as S3.

Preparation of g-C₃N₄/Fe₃O₄ Composite

g-C₃N₄/Fe₃O₄ composites were prepared by using the ultrasonic deposition method. First, 0.30 g of S1 and 0.08 g of iron oxide (Fe₃O₄) were weighed and dissolved with a mixture of 40 mL of methanol and distilled water in a conical flask. The mixture was stirred for 3 hours at room temperature using a

magnetic stirrer. The mixture undergoes ultrasonication for 45 minutes to ensure the mixture is homogeneous. Then, the solution was stirred for another 1 hour and centrifuged for 5 minutes at a rate of 8500 rpm. The supernatant was decanted, and all the resulting pellets were dried using an oven for 8 hours at 60 °C. The samples were labeled as S4. The same procedures were repeated using the S2, and the samples were denoted as S5.

Photocatalytic Degradation

Under visible light irradiation, the photocatalytic degradation reaction of MB in water was carried out. 50 mg of samples were dispersed with continuous stirring into 50 mL of a 10 mg/L dye solution. Before the irradiation, the suspension was stirred in the dark for 30 minutes to allow the adsorption-desorption equilibrium. Next, the solution was exposed to a 18 W UV lamp) for 300 min with constant stirring. Samples of 3 mL were collected at 30 min intervals throughout the experiment. The concentration of MB in the solution was measured using a UV-Vis Spectrophotometer (PerkinElmer Lambda 35) at $\lambda_{max} = 664$ nm, and the photodegradation percentage was evaluated using Equation (1).

$$\text{Degradation (\%)} = \frac{(C_o - C_t)}{C_o} \times 100 \quad (1)$$

where C_o (mg/L) is the initial concentration of MB prior to irradiation and C_t (mg/L) is the concentration of MB after degradation at a specified time interval.

The Langmuir-Hinshelwood (L-H) kinetic model was used to determine the rate of MB photo-degradation as expressed in the following equation:

$$r = \left(\frac{dc}{dt} \right) = k_{app} \quad (2)$$

which can be rewritten as

$$\ln \left(\frac{C_o}{C_t} \right) = k_{app} t \quad (3)$$

where k_{app} is the pseudo-first-order rate constant obtained from the slope of the plot $\ln \left(\frac{C_o}{C_t} \right)$ versus time (t). C_o represent the initial concentration, and C_t is the concentration at a specified time interval (t).

Table 1. Samples code with the composition of all samples

Samples Code	Composition
S1	g-C ₃ N ₄ (using urea as the precursor)
S2	g-C ₃ N ₄ (using a mixture of urea and melamine as the precursor)
S3	Fe ₃ O ₄
S4	g-C ₃ N ₄ /Fe ₃ O ₄ (Composite of g-C ₃ N ₄ (S1) and Fe ₃ O ₄)
S5	g-C ₃ N ₄ /Fe ₃ O ₄ (Composite of g-C ₃ N ₄ (S2) and Fe ₃ O ₄)

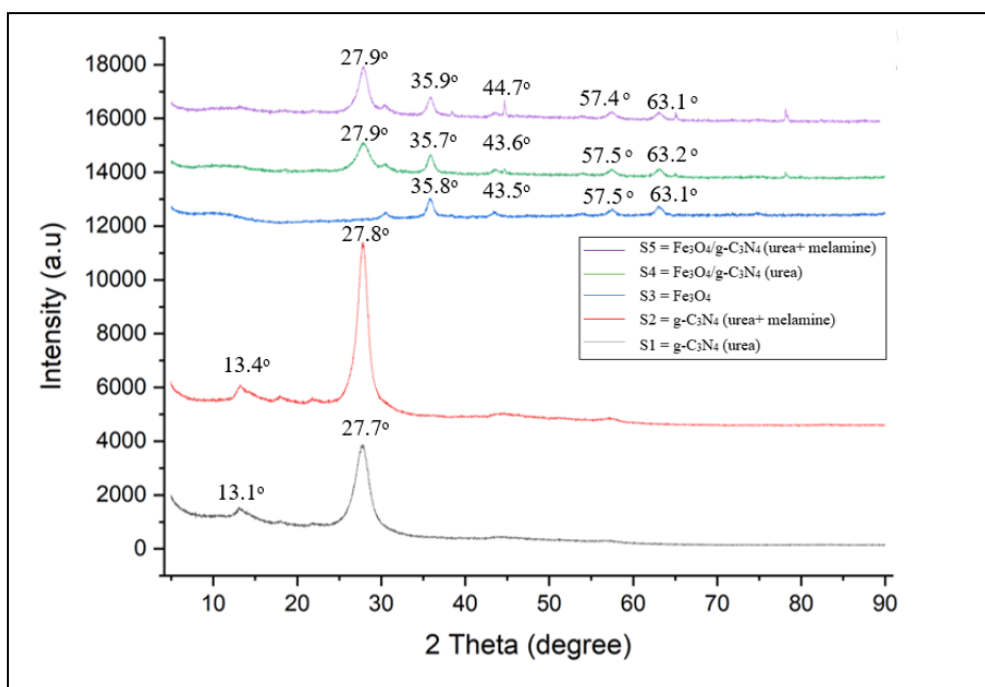


Figure 1. XRD patterns for the $g\text{-C}_3\text{N}_4$ synthesized with different precursors, Fe_3O_4 and $g\text{-C}_3\text{N}_4/\text{Fe}_3\text{O}_4$.

RESULTS AND DISCUSSION

Characterization

Crystallography Analysis

Figure 1 shows the XRD patterns of pure $g\text{-C}_3\text{N}_4$ synthesized using different precursors (S1 and S2), Fe_3O_4 (S3), and magnetic composites of $g\text{-C}_3\text{N}_4/\text{Fe}_3\text{O}_4$ (S4 and S5). XRD of all samples confirms the crystalline phase of pure $g\text{-C}_3\text{N}_4$, Fe_3O_4 , and $g\text{-C}_3\text{N}_4/\text{Fe}_3\text{O}_4$. The apparent strong peak appears approximately at $2\theta = 27.8^\circ$, corresponding to the (002) plane of $g\text{-C}_3\text{N}_4$ (JCPDS 87-1526), which is attributed to the stacking of the conjugate aromatic system of $g\text{-C}_3\text{N}_4$. The weak peak at about $2\theta = 13.1^\circ$ ascribed to the (100) plane is related to the interlayer stacking of the tri-s-triazine motif in-plane nitrogen connections [8, 29]. This indicates the successful synthesis of $g\text{-C}_3\text{N}_4$ via thermal polymerization from urea and a mixture of urea and melamine.

The XRD pattern of S3 revealed the crystalline phase of Fe_3O_4 with six distinctive diffraction peaks at planes $2\theta = (220)$ at 30.6° , (311) at 35.8° , (400) at 43.5° , (422) at 53.3° , (511) at 57.5° and (440) at 63.1° [25, 26]. Samples were indexed to a single-phase cubic structure with $\text{Fd}\bar{3}\text{m}$ space group, and all the diffraction peaks agreed with JCPDS file No.19-0629 (JCPDS). No other distinctive peaks were observed, suggesting the sample's purity. While the diffraction peaks at $2\theta = 36^\circ$, 44° , 57° and 63° in the S4 and S5 composites are associated with the face-centered cubic spinel structure of Fe_3O_4 deposited on $g\text{-C}_3\text{N}_4$. Since there are no additional diffraction peaks, the synthesized

material is entirely a composite of pure magnetite and $g\text{-C}_3\text{N}_4$ combination. The intensity of two plane peaks (100) and (002) of S4 and S5 decreases and becomes broader together with the lattice spacing of the (002) peak increasing from 27.7 to 27.9 , indicating that Fe_3O_4 nanoparticles have closely combined with $g\text{-C}_3\text{N}_4$, and hindered graphitic carbon nitride crystal growth thus changed their growing environment, resulting in magnetic $\text{Fe}_3\text{O}_4/g\text{-C}_3\text{N}_4$ composites.

Functional Group Analysis

The FTIR spectra of pure $g\text{-C}_3\text{N}_4$ synthesized using different precursors, Fe_3O_4 , and magnetic composites of $g\text{-C}_3\text{N}_4/\text{Fe}_3\text{O}_4$ are shown in Figure 2. The peaks appearing in the FITR spectrum were assigned to various groups and bonds in accordance with their respective wavenumbers, including (1) broad peak from 3100 to 3400 cm^{-1} centered at 3183 cm^{-1} corresponding to the stretching vibration of the O-H and N-H groups, which may be due to the unreacted amino groups and adsorbed H_2O [6]; (2) the peaks located between 1200 cm^{-1} to 1600 cm^{-1} are the typical stretching vibration of C-N heterocyclic consisting of C-N and C=N bonds [27]; (3) peak at 808 cm^{-1} correspond to the breathing mode of C-N stretching in triazine rings which is a specific characteristic peak of $g\text{-C}_3\text{N}_4$ [6]; (4) peak at around 509 cm^{-1} corresponding to the stretching vibration of Fe-O in Fe_3O_4 , and (5) the peak of 509 cm^{-1} blueshift to 501 cm^{-1} when the Fe doped into $g\text{-C}_3\text{N}_4$. The presence of peaks at 808 cm^{-1} , between 1200 cm^{-1} to 1600 cm^{-1} , and at 501 cm^{-1} indicates that S4 and S5 are the composites of Fe_3O_4 and $g\text{-C}_3\text{N}_4$. This is in agreement with the results of XRD.

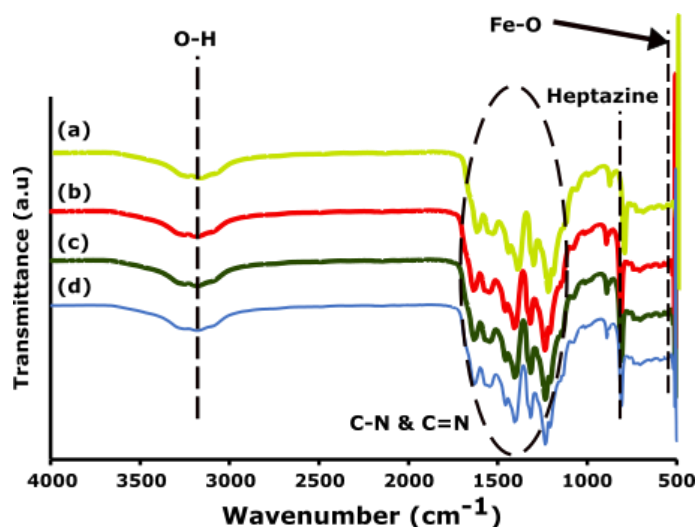


Figure 2. The FTIR spectrum for the (a) S1, (b) S2, (c) S4 and (d) S5.

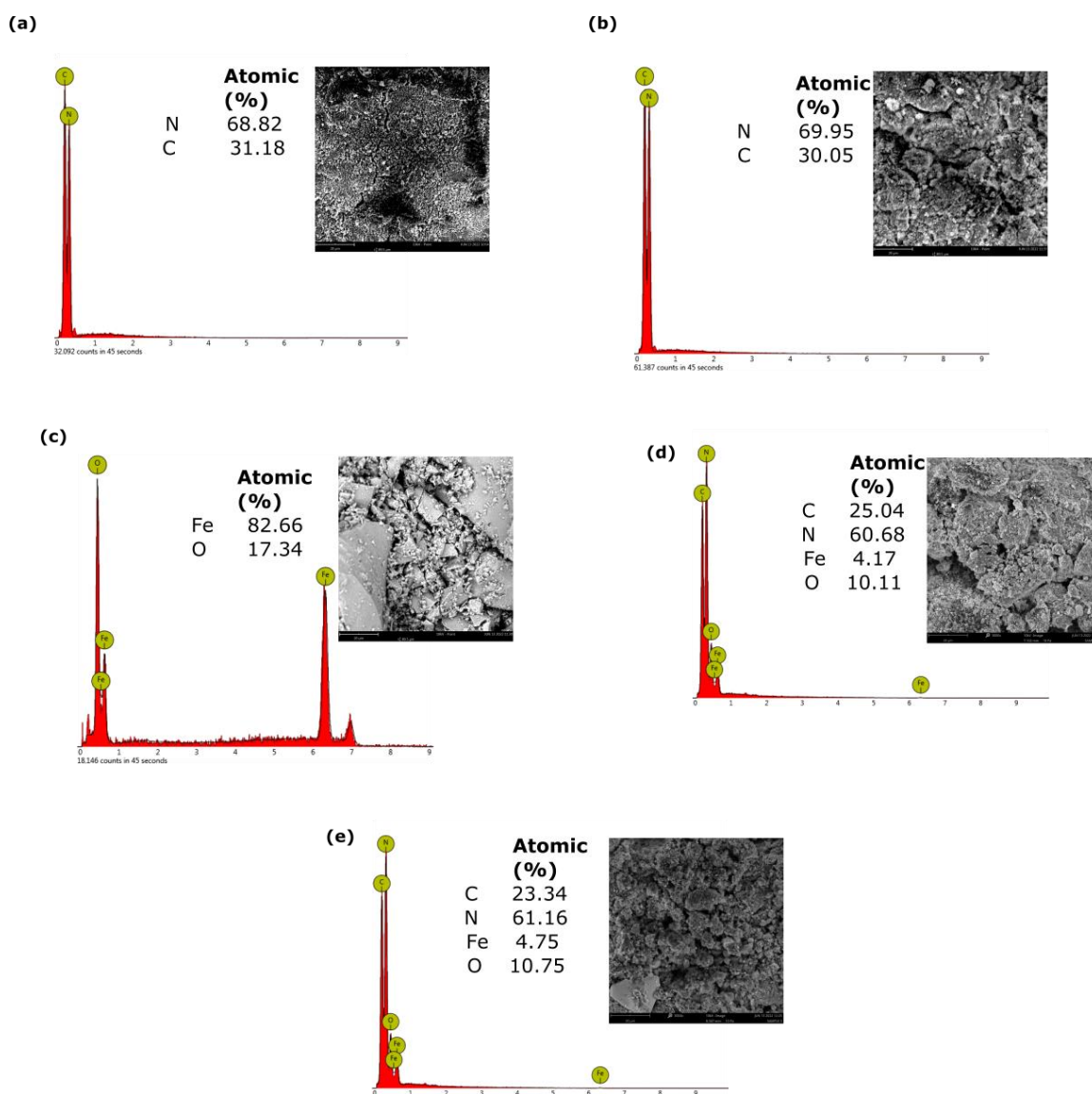


Figure 3. SEM images and EDX spectrum of (a) g-C₃N₄ (S1), (b) g-C₃N₄ (S2), (c) Fe₃O₄ (S3), (d) g-C₃N₄/Fe₃O₄ (S4), (e) g-C₃N₄/Fe₃O₄ (S5).

Morphology and Surface Analysis

EDX analysis was used to determine the purity of the samples, and the findings are depicted in Figure 3. As can be observed, both S1 and S2 are composed of the components C (carbon) and N (nitrogen). The presence of Fe (iron) and O (oxygen) was confirmed by EDX microanalysis. The distinctive peak, observed approximately at 0.6 keV, confirmed the presence of nano crystalline elemental iron. EDX spectra inferred the presence of elements Fe (iron) and O (oxygen) and thus confirmed the chemical composition of Fe_3O_4 nanoparticles in S3. While the composite of S4 and S5 consists of the elements C, N, Fe, and O, indicating it is a combination of $\text{g-C}_3\text{N}_4$ and Fe_3O_4 . No other impurities were detected in all samples.

While the microstructure of S1 and S2 is granular, with rough surfaces observed (Figure 3 (a) and (b)), the surface of the Fe_3O_4 appears (Figure 3 (c)) smoother compared to the $\text{g-C}_3\text{N}_4$ samples. There are no particles on the surface of the Fe_3O_4 that would indicate the absence of other residuals. After combining $\text{g-C}_3\text{N}_4$ with Fe_3O_4 , the material's surface becomes less rough (Figure 3 (d) and (e)), which reveals iron oxide particles are distributed on the surface of $\text{g-C}_3\text{N}_4$, which was consistent with the EDX results.

Optical properties

It is considered that photocatalyst optical characteristics

significantly impact photocatalytic activity. As a result, UV-vis DRS spectra of the resulting samples were provided, and the results are shown below in Figure 4. The absorption edge of samples S1 and S2 are approximately 451 nm corresponding to the band gaps at 2.97 and 2.98 eV, respectively. There are in good agreement with previous reports [30]. The band gaps for composites S4 and S5 are calculated to be 2.87 eV and 2.90 eV, respectively. The values of the composites do not change significantly compared to the band gap of as prepared $\text{g-C}_3\text{N}_4$. It is observed that the band gap value of composites is decreased after doping with Fe_3O_4 , which may be due to the interaction of $\text{g-C}_3\text{N}_4$ and Fe_3O_4 in the composites, which led to more electron-hole pairs under visible light irradiation, which increased photocatalytic activity [31].

Meanwhile, the absorption edge of the magnetic samples (S4 and S5) are further red shifted to the visible range, indicating that the incorporation of the magnetite particles had successfully extended the visible light response of the photocatalyst, as also reported by other researchers [1,2]. The red shift is believed to be triggered by the delocalization of π electrons by the well-connected 2D conjugated planes and the exciton splitting to generate free charges [32]. Generally, a larger range of visible light absorption is favourable for increasing electron and hole pairs and photocatalytic activity. As a result, inserting Fe_3O_4 particles into $\text{g-C}_3\text{N}_4$ may be advantageous for photocatalytic reactions [3].

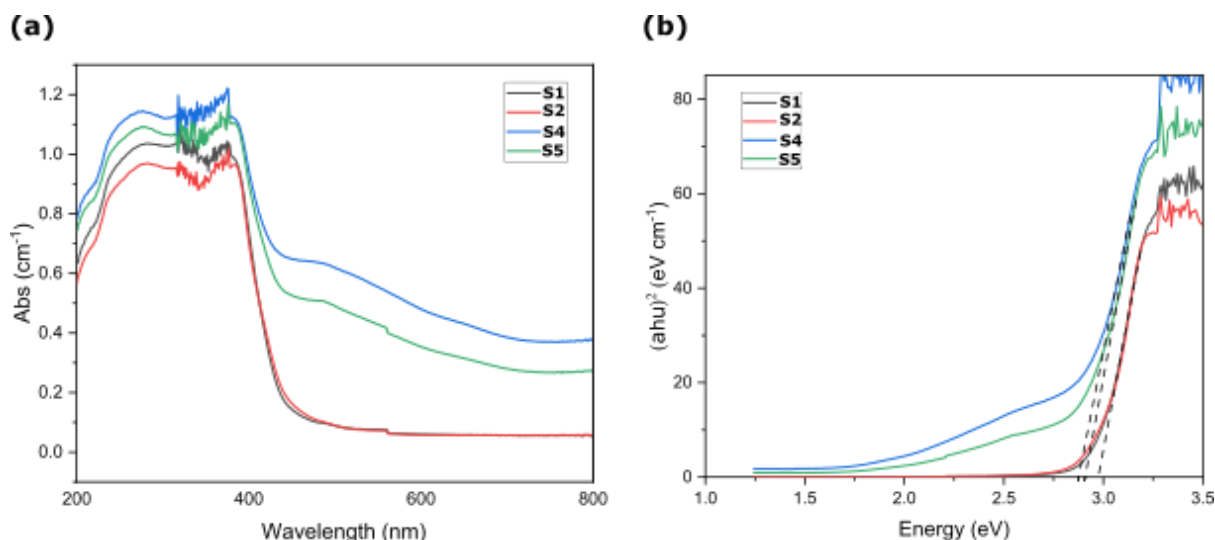


Figure 4. (a) UV-Vis DRS and (b) Plots of $(ahv)^2$ versus $h\nu$ for the $\text{g-C}_3\text{N}_4$ synthesized with different precursors (S1 and S2) and $\text{g-C}_3\text{N}_4/\text{Fe}_3\text{O}_4$ (S4 and S5).

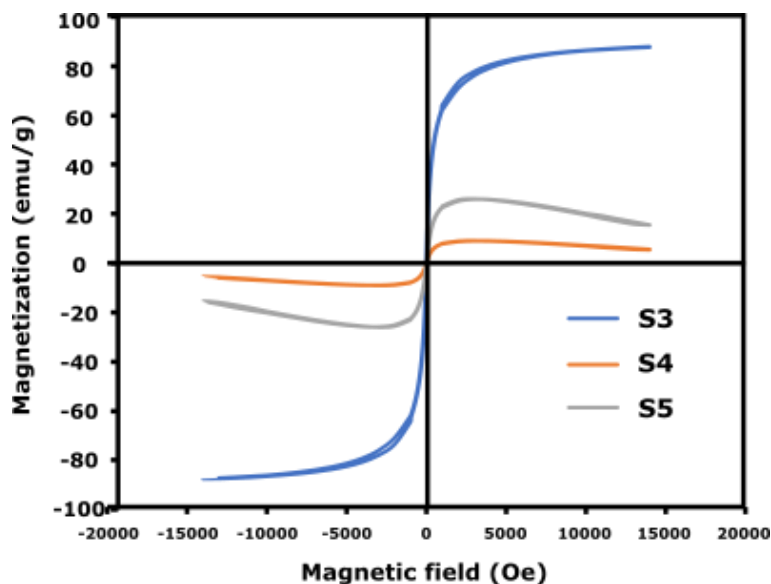


Figure 5. Magnetization curve of S3, S4, and S5 samples at room temperature.

Magnetic Properties

The magnetic properties of all samples are investigated at room temperature. Figure 5 shows the magnetization curves as a function of the applied external magnetic field for pure Fe₃O₄ (S3) and Fe₃O₄/ g-C₃N₄ composites (S4 and S5). The saturation magnetization of Fe₃O₄ nanoparticles is 87.87 emu/g, indicating that the Fe₃O₄ nanoparticles have a high magnetic behavior. The S4 and S5 composite has a lower saturation magnetization than pure Fe₃O₄. The presence of non-magnetic g-C₃N₄ reduces the nano-composite's saturation magnetization. However, S5 has a higher magnetization value than

S4 due to the higher contents of Fe (4.75%) elements compared to S4 (4.15% of Fe) derived from EDX data.

Figure 6 (b) demonstrates that the composites were completely magnetically separated in 30 seconds by placing a magnet near the vessel. These images illustrate that separation (Figure 6 (b)) and redispersion (Figure 6 (a)) of composites may be accomplished simply and rapidly. Although the saturation magnetization of the composite is low, it is high enough to separate the composite from the solution magnetically using an external magnetic force due to its exceptional magnetic property.

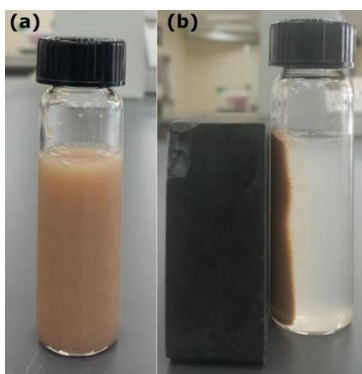


Figure 6. Magnetic behavior of composites towards a neodymium magnet

Table 2. Elemental analysis of all samples.

Sample	Nitrogen (%)	Carbon (%)	Hydrogen (%)	Oxygen (%)
S1	65.23	32.93	1.84	0
S2	64.28	34.12	1.59	0
S3	0.0000	2.26	0.51	97.23
S4	59.14	28.01	1.76	11.00
S5	63.26	29.78	1.52	5.44

Elemental Analysis

As seen in Table 2, in addition to carbon and nitrogen, all samples contained a small amount of hydrogen. Small amounts of additional hydrogen and oxygen may be derived from the residual unreacted amino group and absorbed water of the sample. Some CN_x materials reportedly have a great propensity to absorb water from the environment [33]. As can be seen, the g-C₃N₄ sample consists of C and N elements in the compound [5]. The g-C₃N₄/Fe₃O₄ composite comprises lower contents of C, N, and H elements, especially the C content, demonstrating further the presence of Fe₃O₄ in the composite, which is consistent with EDX data.

Photodegradation Activity

Figure 7 (a) shows the photodegradation of MB by the synthesized magnetic composites using a UV-vis spectrophotometer. After 30 minutes of stirring, dark adsorption equilibrium was reached between MB solution and magnetic composites and subsequently for 300 min with the presence of composites and UV light. No photodegradation of MB was observed when the experiments were conducted under dark conditions. MB deteriorated by 10% after 300 min of visible-light irradiation in a blank experiment without a photo-

catalyst. The photolysis of MB was also negligible, showing the MB stability under UV light. After 300 min of irradiation, the MB degradation of S1 reaches 27.4%, whereas those of S2 reach 40.5%. Meanwhile, the magnetic composite S4 and S5 enable 68.9% and 90.9% degradation of MB within 5 hours, respectively.

Figure 7 (b) shows the MB degradation rate constants obtained using a pseudo-first-order kinetic model. This reaction successfully followed the pseudo-first-order reaction and confirmed that no adsorption process occurred. The degradation reaction rate constant over the S1, S2, S4 and S5 composites is $1.0 \times 10^{-3} \text{ min}^{-1}$, $1.4 \times 10^{-3} \text{ min}^{-1}$, $4.0 \times 10^{-3} \text{ min}^{-1}$ and $8.3 \times 10^{-3} \text{ min}^{-1}$, respectively (see Table 3). This study demonstrates that the degradation of MB is approximately two times greater when a mixture of urea and melamine is used as the g-C₃N₄ precursor than urea alone.

It was evident that the photocatalytic degradation abilities of g-C₃N₄ synthesized from different precursors give different degradation abilities for MB. This may be attributed to the different compositions of the samples, surface morphology, and optical properties, as indicated in characterization data [7, 8].

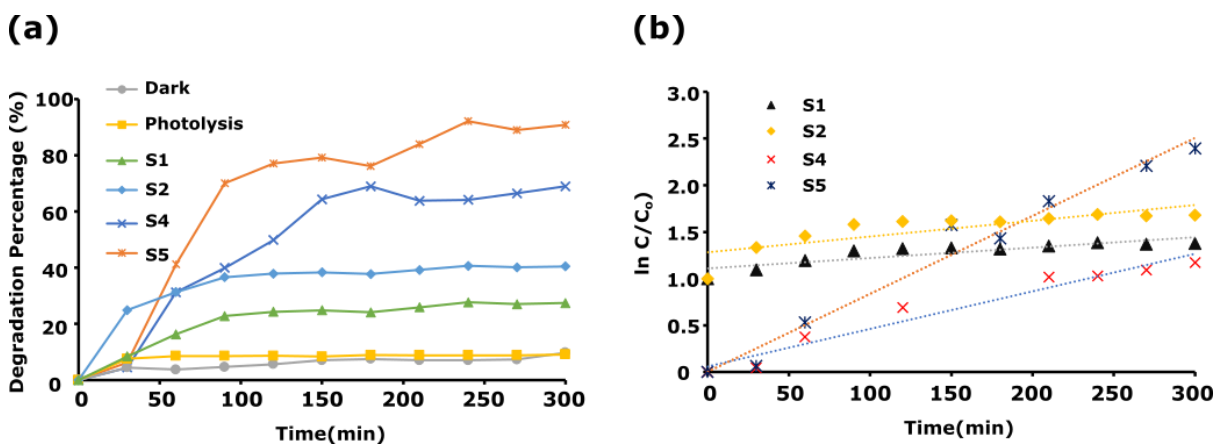


Figure 7. (a) Degradation percentage (%) and (b) Kinetics of the removal of MB by prepared samples

Table 3. Kinetic data for MB photocatalytic degradation of the prepared magnetic composites

Sample	Photocatalytic kinetics	
	$k_{app} \times 10^{-3} \text{ (min}^{-1}\text{)}$	R^2
S1	1.0	0.8937
S2	1.4	0.7666
S4	4.0	0.9541
S5	8.3	0.9736

CONCLUSION

Graphitic carbon nitride (g-C₃N₄) was successfully prepared using urea or a mixture of urea and melamine via the thermal polymerization method. FTIR analysis indicated the presence of respective stretching vibrations of g-C₃N₄. Then, the g-C₃N₄ was loaded with Fe₃O₄ to obtain magnetic composites with high saturation magnetization, which suggests that the photocatalyst can be easily separated from the treated solution using a magnetic field. S5 samples show a high percentage degradation (90.9%) of 10 mg/L of MB solution with a rate constant of 8.3 x 10⁻³ min⁻¹.

ACKNOWLEDGEMENTS

The authors gratefully acknowledge the services and facilities provided by the Institute of Science, UiTM Shah Alam, and the Faculty of Applied Sciences, Tapah Campus, to carry out the laboratory work. Appreciation also goes to Kurita Water and Research Foundation for the research funding (100-TNCPI/INT 16/6/2 (075/2022).

REFERENCES

1. Maleki, A., Hamesadeghi, U., Daraei, H., Hayati, B., Najafi, F., McKay, G., Rezaee, R. (2017) Amine functionalized multi-walled carbon nanotubes: single and binary systems for high capacity dye removal. *Chemical Engineering Journal*, **313**, 826–835.
2. Rauf, M. A., Ashraf, S. S. (2012) Survey of recent trends in biochemically assisted degradation of dyes. *Chemical engineering journal*, **209**, 520–530.
3. Robinson, T., McMullan, G., Marchant, R., Nigam, P. (2001) Remediation of dyes in textile effluent: a critical review on current treatment technologies with a proposed alternative. *Bioresource technology*, **77**, 247–255.
4. Sinar Mashuri, S. I., Ibrahim, M. L., Kasim, M. F., Mastuli, M. S., Rashid, U., Abdullah, A. H., Islam, A., Asikin Mijan, N., Tan, Y. H., Mansir, N. (2020) Photocatalysis for organic wastewater treatment: From the basis to current challenges for society. *Catalysts*, **10**, 1260.
5. Chen, J., Xiong, Y., Duan, M., Li, X., Li, J., Fang, S., Qin, S., Zhang, R. (2019) Insight into the synergistic effect of adsorption–photocatalysis for the removal of organic dye pollutants by Cr-doped ZnO. *Langmuir*, **36**, 520–533.
6. Nguyen, T. K. A., Pham, T. -T., Nguyen-Phu, H., Shin, E. W. (2021) The effect of graphitic carbon nitride precursors on the photocatalytic dye degradation of water-dispersible graphitic carbon nitride photocatalysts. *Applied Surface Science*, **537**, 148027.
7. Mousavi, M., Habibi-Yangjeh, A. (2016) Magnetically separable ternary g-C₃N₄/Fe₃O₄/BiOI nanocomposites: novel visible-light-driven photocatalysts based on graphitic carbon nitride. *Journal of colloid and interface science*, **465**, 83–92.
8. Mousavi, M., Habibi-Yangjeh, A., Abitorabi, M. (2016) Fabrication of novel magnetically separable nanocomposites using graphitic carbon nitride, silver phosphate and silver chloride and their applications in photocatalytic removal of different pollutants using visible-light irradiation. *Journal of colloid and interface science*, **480**, 218–231.
9. Che, Y., Liu, Q., Lu, B., Zhai, J., Wang, K., Liu, Z. (2020) Plasmonic ternary hybrid photocatalyst based on polymeric gC 3 N 4 towards visible light hydrogen generation. *Scientific reports*, **10**, 1–12.
10. de Oliveira Jorgetto, A., Milbrat, A., Schneider, J. F., Li, Z., Giammaria, G., Saeki, M. J., Gianeti, T. M. R., Lima, G. P. P., de Albuquerque Pedrosa, V., Mul, G. (2018) Magnetically-extractable hybrid of magnetite, mesoporous silica and titania for the photo-degradation of organic compounds in water. *Applied surface science*, **457**, 121–133.
11. Md Fauzi, M. A. F., Razali, M. H., Osman, M. U., Mohd Azam, B. (2022) Synthesis and characterisation of TiO₂/g-C₃N₄ as photocatalyst for photodegradation of dyes, phenol and caffeine. *Advances in Materials and Processing Technologies*, 1–21.
12. Razali, M. H., Md Fauzi, M. A. F., Mohd Azam, B., Yusoff, M. (2022) g-C₃N₄/TiO₂ nanocomposite photocatalyst for methylene blue photo-degradation under visible light. *Applied Nanoscience*, 1–10.
13. Huang, Y., Wang, Y., Bi, Y., Jin, J., Ehsan, M. F., Fu, M., He, T. (2015) Preparation of 2D hydroxyl-rich carbon nitride nanosheets for photocatalytic reduction of CO₂. *RSC Advances*, **5**, 33254–33261.
14. Savateev, A., Dontsova, D. (2016) Baking ‘crumbly’ carbon nitrides with improved photocatalytic properties using ammonium chloride. *RSC advances*, **6**, 2910–2913.
15. Zhang, Y., Yuan, J., Ding, Y., Liu, B., Zhao, L., Zhang, S. (2021) Research progress on g-C₃N₄-based photocatalysts for organic pollutants degradation in wastewater: From exciton and carrier perspectives. *Ceramics International*, **47**, 31005–31030.
16. Mirzaei, A., Chen, Z., Haghghat, F., Yerushalmi, L. (2019) Magnetic fluorinated mesoporous g-

- C3N4 for photocatalytic degradation of amoxicillin: transformation mechanism and toxicity assessment. *Applied Catalysis B: Environmental*, **242**, 337–348.
17. Lima, M. J., Sampaio, M. J., Silva, C. G., Silva, A. M., Faria, J. L. (2019) Magnetically recoverable Fe₃O₄/g-C₃N₄ composite for photocatalytic production of benzaldehyde under UV-led radiation. *Catalysis Today*, **328**, 293–299.
 18. Taib, N. I., Woodward, R. C., Pierre, T. G. S., Iyer, K. S. (2022) Chain Formation of PNIPAM-Coated Magnetic Nanoparticles in an External Magnetic Field and the Effect of Temperature. *IEEE Transactions on Magnetics*, **58**, 1–5.
 19. Taib, N. I., Woodward, R. C., Pierre, T. G. S. (2022) The Effect of Silica Shell Thickness on Magnetic and Proton Relaxometric Properties: Fe₃O₄@mSiO₂ Nanoparticles. *IEEE Transactions on Magnetics*, **58**, 1–7.
 20. Jacinto, M., Ferreira, L., Silva, V. (2020) Magnetic materials for photocatalytic applications—a review. *Journal of Sol-Gel Science and Technology*, **96**, 1–14.
 21. Wang, J., Shao, X., Liu, J., Zhang, Q., Ji, X., Tian, G. (2020) Mesoporous magnetic g-C₃N₄ nanocomposites for photocatalytic environmental remediation under visible light. *Ecotoxicology and Environmental Safety*, **205**, 111147.
 22. Köwitsch, I., Mehring, M. (2021) Coatings of magnetic composites of iron oxide and carbon nitride for photocatalytic water purification. *RSC advances*, **11**, 14053–14062.
 23. Christoforidis, K. C., Montini, T., Bontempi, E., Zafeiratos, S., Jaén, J. J. D., Fornasiero, P. (2016) Synthesis and photocatalytic application of visible-light active β-Fe₂O₃/g-C₃N₄ hybrid nanocomposites. *Applied Catalysis B: Environmental*, **187**, 171–180.
 24. Kheradmand, A., Wainwright, A., Wang, L., Jiang, Y. (2020) Anchoring iron oxides on carbon nitride nanotubes for improved photocatalytic hydrogen production. *Energy & Fuels*, **35**, 868–876.
 25. Taib, N. I., Latif F. A., Mohamed, Z., Zambri, N. D. S. (2018) Green synthesis of iron oxide nanoparticles (Fe₃O₄-NPs) using *Azadirachta indica* aqueous leaf extract. *International Journal of Engineering & Technology*, **7**, 9–13.
 26. Zambri, N. D. S., Taib, N. I., Abdul Latif, F., Mohamed, Z. (2019) Utilization of neem leaf extract on biosynthesis of iron oxide nanoparticles. *Molecules*, **24**, 3803.
 27. Zhang, X., Ren, B., Li, X., Xu, Y., Liu, B., Yu, P., Sun, Y., Mei, D. (2021) Efficiently enhanced visible-light photocatalytic activity by in situ deposition of Ag@ AgBr on g-C₃N₄/Fe₃O₄ magnetic heterogeneous materials. *Separation and Purification Technology*, **254**, 117596.
 28. Mohanraj, J., Durgalakshmi, D., Saravanan, R. (2021) Water-soluble graphitic carbon nitride for clean environmental applications. *Environmental Pollution*, **269**, 116172.
 29. You, J., Bao, W., Wang, L., Yan, A., Guo, R. (2021) Preparation, visible light-driven photocatalytic activity, and mechanism of multiphase CdS/C₃N₄ inorganic-organic hybrid heterojunction. *Journal of Alloys and Compounds*, **866**, 158921.
 30. Fu, J., Yu, J., Jiang, C., Cheng, B. (2018) g-C₃N₄-Based heterostructured photocatalysts. *Advanced Energy Materials*, **8**, 1701503.
 31. Zhou, X., Jin, B., Chen, R., Peng, F., Fang, Y. (2013) Synthesis of porous Fe₃O₄/g-C₃N₄ nanospheres as highly efficient and recyclable photocatalysts. *Materials Research Bulletin*, **48**, 1447–1452.
 32. Zheng, D., Pang, C., Liu, Y., Wang, X. (2015) Shell-engineering of hollow gC₃N₄ nanospheres via copolymerization for photocatalytic hydrogen evolution. *Chemical Communications*, **51**, 9706–9709.
 33. Zambov, L. M., Popov, C., Abedinov, N., Plass, M. F., Kulisch, W., Gotszalk, T., Grabiec, P., Rangelow, I. W., Kassing, R. (2000) Gas-Sensitive Properties of Nitrogen-Rich Carbon Nitride Films. *Advanced Materials*, **12**, 656–660.